Results in Engineering 16 (2022) 100624

Contents lists available at ScienceDirect

Results in Engineering

journal homepage: www.sciencedirect.com/journal/results-in-engineering

Hard-core/zeolitized-shell beads obtained by surface zeolitization of activated clay particles

Claudia E. Rivera Enríquez [a], Maximiliano R. Gonzalez [b,*], Facundo Barraqué [c], Andrea M. Pereyra [b,d], Elena I. Basaldella [b]

[a] Facultad de Estudios Superiores Cuautitlán, Universidad Nacional Autónoma de México (UNAM), Av. Primero de Mayo S/N, Sta. María Guadalupe las Torres, 54740, Edo. de México, Mexico
[b] Centro de Investigación y Desarrollo en Ciencias Aplicadas Dr. J.J. Ronco (CINDECA) (CONICET-CIC-UNLP), 47 N°257, B1900 AJK, La Plata, Argentina
[c] Centro de Tecnología de Recursos Minerales y Cerámica (CETMIC), Argentina, Cno. Centenario y 506, Gonnet, B1897, La Plata, Argentina
[d] Universidad Tecnológica Nacional-Facultad Regional La Plata, 60 y 124, La Plata, Argentina

ARTICLE INFO

Keywords:
Clay
Calcination
Alkaline activation
Hydrothermal synthesis
Hard-core/zeolitized-shell

ABSTRACT

This work presents a novel and cost-effective procedure that improves the reactivity of kaolinitic clay particles toward the generation of millimetric hard-core/zeolitized-shell units. The obtained particulate material is ready to use as ion exchanger beads in a fixed adsorption bed. Starting from properly activated, millimeter-sized clay units, the transition of their external surface towards a new crystalline ordering could be induced. The Na_2CO_3 alkaline activation treatment applied to previously calcined clay particles allowed obtaining different levels of $NaAlSiO_4$ polymorphs on the external surface of the particles, which are easily transformed to zeolitic products. By varying the synthesis conditions, FAU and LTA zeolite structures were successfully obtained on the surface of hardened particles, reaching conversions close to 90%. The starting clay, pretreated clays, and products obtained after hydrothermal synthesis were characterized by X-ray diffraction (XRD), scanning electron microscopy (SEM), and energy dispersive X-ray microanalysis (EDX). The versatility of the method is exemplified in obtaining adsorbents specifically designed for the retention of Cd^{2+} and Ni^{2+} contaminating ions. A total removal of Cd^{2+} and Ni^{2+} was achieved at 150 min from initial 40 ppm solutions, being 98% and 94% from initial 120 ppm solutions for cadmium and nickel, respectively.

1. Introduction

Zeolites are microporous materials mainly consisting of an ordered arrangement of $[SiO_4]^{4-}$ and $[AlO_4]^{5-}$ tetrahedral entities. Zeolitic frameworks contain channels and cavities commonly occupied by exchangeable alkali and/or alkaline earth cations such as Na^+, K^+, and Ca^{2+} [1]. Different synthesis procedures have been used to transform aluminosiliceous materials into zeolite structures, those involving hydrothermal or microwave treatments being the most usual [2–5]. Besides, low-cost raw materials such as kaolin clays, fly ash, volcanic ash, waste glass, and rice husk, among others, could be efficiently used for obtaining zeolite products [6–10]. Using these nonconventional starting materials, an important challenge is to improve their conversion into zeolite-type structures by applying different activation treatments aimed at achieving an increase in their intrinsic reactivity and minimizing the presence of non-zeolitic phases in the final product.

Furthermore, excessive and improper use of water causes the degradation of natural environments, turning them into inadequate sources for satisfying social, commercial, and agricultural human needs [11,12]. The current water crisis highlights the lack of basic sanitation in water treatment, limiting its access to populations and spreading diseases [13]. Therefore, it is important to improve the existing water purification treatments by developing affordable and accessible purification techniques.

The unique properties of zeolites such as ion exchange, adsorption, thermal stability, and porous structure make them suitable for being used in the development of a multiplicity of novel technologies. Among them, it is possible to highlight the synthesis of advanced solids or membranes for water and air purification [14–18]. The first step in the most common methodologies used for obtaining zeolitic adsorbent materials consists of the hydrothermal synthesis of a micrometer-sized powder formed by zeolitic individual crystals or small agglomerates.

* Corresponding author.
E-mail address: maximi_gonz@yahoo.com.ar (M.R. Gonzalez).

https://doi.org/10.1016/j.rineng.2022.100624
Received 20 July 2022; Received in revised form 30 August 2022; Accepted 30 August 2022
Available online 6 September 2022

Table 1
Sequential treatment conditions.

Treatment	Time	Temperature and samples			
Heat treatment	2 h	800 °C C1	960 °C C2	1100 °C C3	1200 °C C4
Alkaline activation	2 h	800 °C C5	800 °C C6	800 °C C7	800 °C C8

The subsequent step is to form the powder into pellets or beads of various sizes to ensure the packing of fixed beds during wastewater treatment processes [19]. However, obtaining low-cost, macroscopic, attrition-resistant and high zeolitized particles is a challenging task [20].

In this work, a methodology for the surface zeolitization of millimetric kaolin particles from clay deposits located in Buenos Aires Province, Argentina, was proposed. A selected millimeter-sized fraction of the raw clay was submitted to a series of thermal and hydrothermal treatments in order to obtain a zeolitized surface layer grown onto a hard clay core. The proposed methodology seems to be appropriate for obtaining kaolin-based adsorbent beads for packed-bed columns, avoiding the crystal agglomeration step. The novelty of the proposed method is based on the use of a low-cost natural clay to obtain a millimeter-sized adsorbent product, ready to use as a cation exchanger in packed-bed columns, avoiding the need to form spheres or pellets by extrusion.

2. Experimental

2.1. Raw material

Granulated clay from kaolinitic deposits, located in Tandil, Buenos Aires, Argentina, was used as raw material. The clay was sieved, and the fraction with particle size between 4.76 and 8 mm was separated from the bulk. These natural clay grains were designated as sample C0. The chemical composition was obtained by EDX.

2.2. Pretreatments and hydrothermal synthesis

2.2.1. Calcination and alkaline activation

For increasing both the hardness and the reactivity toward zeolite crystallization of the clay, the C0 sample was submitted to two sequential steps: calcination and alkaline activation.

In the first instance, C0 fractions were heat-treated in static conditions (5 °C/min) for 2 h at different temperatures: 800 °C, 960 °C, 1100 °C, and 1200 °C. The samples were named C1, C2, C3, and C4, respectively.

Subsequently, the reactivity of the clay samples was increased by alkaline fusion using 50 wt% Na_2CO_3 (Biopack, p.a.). The mixtures of calcined clay and Na_2CO_3 were homogenized by sonication for 400 s, and then heat-treated at 800 °C for 2 h (5 °C/min) [21]. The activated samples were labelled as C5, C6, C7, and C8, respectively. Table 1 summarizes the identification of the samples and the treatment conditions.

2.2.2. Hydrothermal synthesis

Each activated sample (5 g) was placed in contact with the synthesis solution in a polypropylene reactor, under stirring (30 min), and aged at room temperature for 48 h without stirring. The Al/Si ratio of the synthesis mixture was adjusted considering that the Al^{3+} and Si^{4+} amounts present in the clay were completely available. In order to obtain the two most representative zeolitic adsorbents, NaA and NaX, the corresponding synthesis mixtures with the adequate stoichiometry were prepared (reaction mixture A and reaction mixture X respectively). The selected molar ratios were obtained by adding the suitable amounts of reagents such as NaOH (Carlo Erba), deionized water, and $NaAlO_2$ (commercial Alum powder, 36.5% Al_2O_3, 29.6% Na_2O, 33.9% H_2O).

Afterwards, the synthesis mixtures were placed in a conventional air oven at the selected temperature (90 °C for mixture X and 100 °C for mixture A). The progress of the synthesis was followed by taking aliquots at different reaction times (3, 6, and 16 h). The obtained samples were washed with deionized water and dried in a conventional air oven at 50 °C. Table 2 summarizes the synthesis conditions and nomenclature used for labeling each of the samples taken during the hydrothermal synthesis.

2.3. Cation exchange process

The zeolitized sample with the highest content of zeolite A (sample $C5A_{6h}$) was used to evaluate its efficiency as ion scavenger in the purification of aqueous solutions contaminated with Cd^{2+} and Ni^{2+} species. Solutions were prepared using cadmium chloride 1-hydrate ($CdCl_2{\cdot}H_2O$, Biopack) or nickel sulfate 6-hydrate ($NiSO_4{\cdot}6H_2O$, Biopack). The ion exchange experiments were carried out at two different solid/liquid ratios (S/L), by adding 1 or 3 g of zeolitized clay to 1000 mL of cadmium or nickel solutions containing 40 and 120 ppm, respectively. Each cation exchange was carried out at 25 °C using an uncovered batch reactor made of polypropylene under continuous slight stirring, taking samples at different exchange times. The evolution of the pH value of the exchange solution was recorded for each of the different tests. The obtained samples were filtered, and the concentration of cadmium and nickel in the liquid phase was determined by atomic absorption spectroscopy (AAS). The removal efficiency was calculated.

$$Removal\ effiency = \frac{C0 - C1}{C0}\ x\ 100\%$$

where C0 is the initial heavy metal cation concentration (ppm) and C1 is the residual heavy metal cation concentration after cation exchange at a determined time (ppm).

2.4. Physicochemical characterization

The mineralogical compositions of C0, its pretreated/activated derived samples, as well as those corresponding to the products obtained at different times during the hydrothermal synthesis, were determined by XRD. Diffraction patterns were obtained from 5 to 40 °2θ using a Philips PW3710 powder diffractometer with CuKα radiation of 1.5406 Å, using a step width of 0.04°2θ, step time of 10 s, and a Ni-filter. Compound identification was performed using Match! and Jade MDI

Table 2
Synthesis conditions and nomenclature used for identifying the samples during the hydrothermal crystallization.

		Time (h)	SiO_2/Al_2O ratio	Na_2O/H_2O ratio	Na_2O/Al_2O_3 ratio	Samples			
Hydrothermal synthesis	Mixture X	0	6	0.03	9.8	$C5X_{0h}$	$C6X_{0h}$	$C7X_{0h}$	$C8X_{0h}$
		3	6	0.03	9.8	$C5X_{3h}$	$C6X_{3h}$	$C7X_{3h}$	$C8X_{3h}$
		6	6	0.03	9.8	$C5X_{6h}$	$C6X_{6h}$	$C7X_{6h}$	$C8X_{6h}$
		16	6	0.03	9.8	$C5X_{16h}$	$C6X_{16h}$	$C7X_{16h}$	$C8X_{16h}$
	Mixture A	0	1.4	0.03	3.4	$C5A_{0h}$	$C6A_{0h}$	$C7A_{0h}$	$C8A_{0h}$
		3	1.4	0.03	3.4	$C5A_{3h}$	$C6A_{3h}$	$C7A_{3h}$	$C8A_{3h}$
		6	1.4	0.03	3.4	$C5A_{6h}$	$C6A_{6h}$	$C7A_{6h}$	$C8A_{6h}$
		16	1.4	0.03	3.4	$C5A_{16h}$	$C6A_{16h}$	$C7A_{16h}$	$C8A_{16h}$

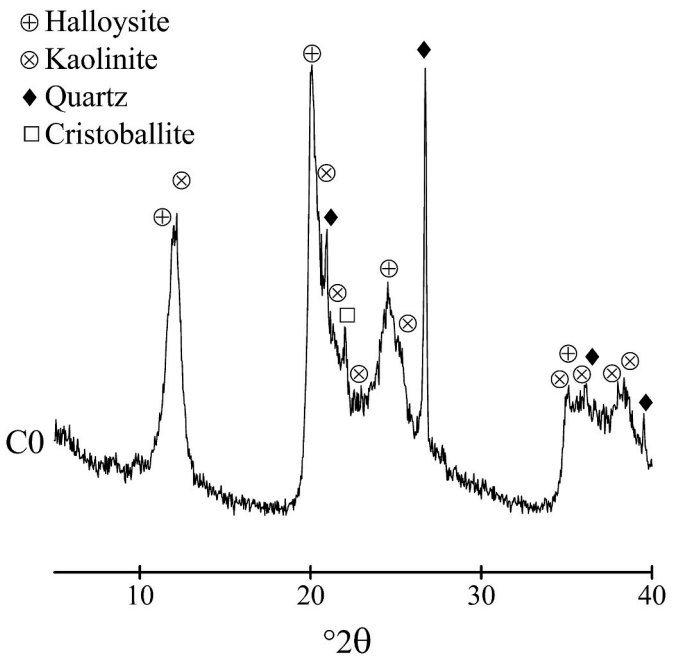

Fig. 1. X-ray diffraction patterns of natural clay, sample C0.

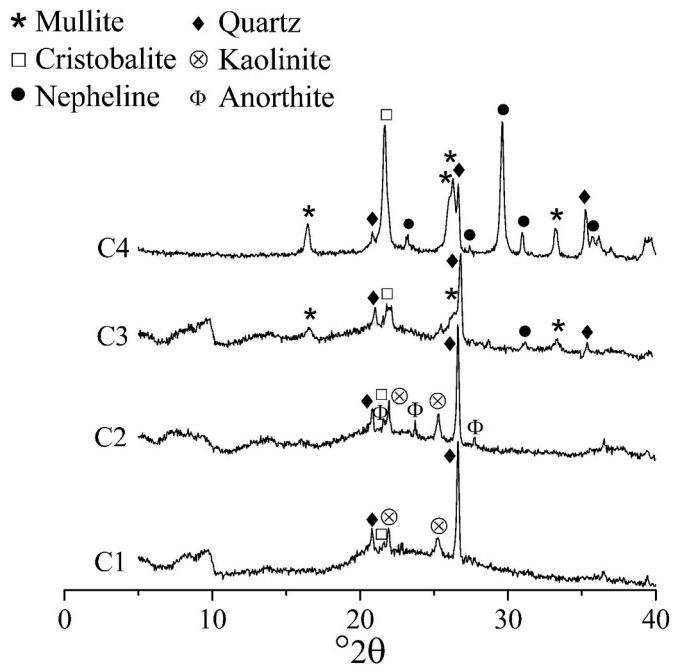

Fig. 2. X-ray diffraction patterns of C0 after being heat-treated at different temperatures.

software. The XRD patterns for Rietveld refinements were acquired from 5 to 80 °2θ using a Bruker Advance D8 powder diffractometer with CuKα radiation of 1.5406 Å, using a step width of 0.02°2θ, step time of 0.5 s, and a Ni-filter. The Rietveld method [22] was performed using TOPAS 6 software to obtain the quantitative percentages of the crystalline components in the different solid samples analyzed. The crystalline phases and zeolite types were determined by comparing diffraction profiles with published data (PDF, Powder Diffraction File). Using the Rietveld refinement, the wt% crystalline composition of the samples was determined. An initial model for Rietveld refinement was built using crystallographic data from the Structure Commission of the International Zeolite Association (IZA-SC) and Crystallography Open Database (COD). According to the crystalline compounds identified in the X-ray diffraction patterns, the following crystallographic information files were used as a starting point: zeolite LTA NaA hydrated, zeolite FAU NaX hydrated, and zeolite Na-P1 hydrated from IZA-SC; nepheline (ID 8104311), mullite (ID 9010159), anatase (ID 1530151), quartz (ID 9009666), and hydroxysodalite (ID 1536465) from COD.

Furthermore, particle size and morphology were determined by using a Philips 505 scanning electron microscope (SEM). The semi-quantitative chemical analysis composition of the starting material was carried out by EDX using an EDX Prime 10 Spectrometer.

3. Results and discussion

3.1. Natural clay

The X-ray diffraction pattern of the natural clay (C0) showed the reflections of hydroxylated aluminosilicates ($Al_2Si_2O_5(OH)_4.nH_2O$) such as halloysite (PDF# 29-1487) and kaolinite (PDF# 80-0885). The reflections of quartz (PDF# 83-2465) and cristobalite (PDF# 82-1403) were also detected (Fig. 1). The C0 pattern presented width-varying reflections, indicative of a sample having a dissimilar degree of crystallinity or nonuniform crystallite size. Additionally, the background between 17 and 30 °2θ indicated the coexistence of an amorphous phase.

The composition (wt%) estimated by EDX chemical analysis was $SiO_2 = 61.9$; $Al_2O_3 = 36.4$; $TiO_2 = 1.5$; and $CaO = 0.2$.

3.2. Pretreatment

3.2.1. Calcination

The crystalline composition of the original clay, sample C0, was notoriously altered by the heat treatment. Fig. 2 shows the X-ray diffraction patterns of the samples C1, C2, C3, and C4 obtained after C0 calcination at 800, 960, 1000, and 1200 °C, respectively. Depending on the temperature, the calcination produced a collapse of the lattice order that increased the amorphous fraction or a topotactic transformation of the natural clay to a new crystalline configuration.

At 800 °C, the complete dehydroxylation of halloysite to give rise to a disordered sheet-like structure was observed [23]. Up to 960 °C, kaolinite was still present, but a decrease in the characteristic reflections occurred. This resistance to dehydroxylation could be attributed to the reaction mechanism being controlled by the thermal diffusion into the kaolinitic structure. The defective nature of clay, indicated by the width of the kaolinite reflections in the X-ray diffraction pattern (Fig. 1), would explain why the heat transfer in the boundary layer outside the crystallites becomes the dehydroxylation rate-limiting factor.

Thus, the increase of background (amorphous halo) in the angular region $1 < 2\theta^\circ < 30$ up to 960 °C was produced by dehydroxylation of halloysite and also by a fraction of kaolinite, which was transformed into disordered structures or metastructures. Close to 960 °C, the appearance of a harder structure corresponding to amorphous premullite, which could also contribute to an increase in the amorphous phase, was also expected [2,23]. Besides, cristobalite (PDF# 82-1403) from natural clay and anorthite (PDF# 71-0788) reflections were present in this range of temperature.

Furthermore, from 1100 °C, new diffraction peaks were identified as mullite (PDF# 74-2419) and nepheline (PDF# 35-0424). At this temperature, the decrease in quartz reflection intensities could be attributed to the transition towards cristobalite. The mechanism of the change from β-quartz to cristobalite is not fully known, but according to Ref. [24] the transformation starts from 1300 °C through an amorphous intermediate state produced by the breaking of the bonds in quartz, followed by the complete transition to cristobalite at about 1700 °C. Nevertheless, in our studies cristobalite formation was detected from 1100 °C. This fact could be explained on the basis that alkaline cations such as Ca^{2+} present in

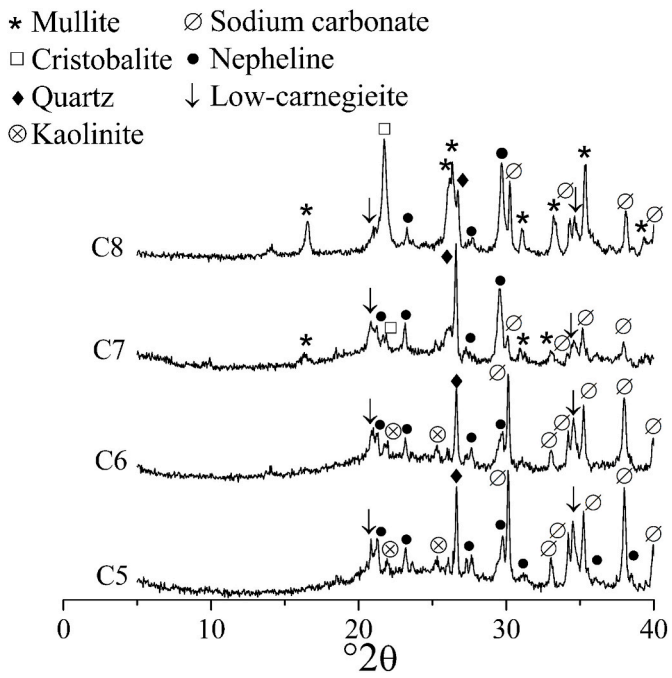

Fig. 3. Diffraction patterns after alkaline fusion with Na_2CO_3 of samples C5, C6, C7, and C8.

the natural clay could catalyze the transformation from quartz to cristobalite. According to Ref. [25], alkaline compounds start melting at a temperature well below the melting point of silica, and the phase transition occurs through a fluid-mediated reaction. These liquids spread into the solid phase, leading to an accelerated decomposition of quartz along with a rapid nucleation and growth of cristobalite.

The nucleation of harder structures was due to the contribution of the amorphous phase. Non-crystalline -Al-O-Si- groupings act as intermediate towards the polymorphic transformation of cubic mullite and hexagonal nepheline, in a process that confirms the topotactic concept in kaolinite transformation [26]. Reflections corresponding to these crystalline species (cristobalite, mullite, and nepheline) became clearer and more intense once the thermal pretreatment reached 1200 °C. The solid-solid transformation of quartz into cristobalite was corroborated by the decrease in the intensities of the peaks at °2θ = 21 and 26. Then, the increase in crystallinity of the solid at this temperature could be attributed to a solid-solid transformation, in which mullite and nepheline continue to grow at the expense of meta-aluminosiliceous species.

3.2.2. Alkaline activation

C1, C2, C3, and C4 were subjected to alkaline activation for 2 h at 800 °C. The X-ray diffraction patterns recorded after this process are shown in Fig. 3.

The samples previously heat-treated at relatively low temperatures (C5 and C6) showed the formation of nepheline and low-carnegieite (PDF# 11-0221) after activation with Na_2CO_3. Those pretreated at higher temperatures (samples C7 and C8) produced low-carnegieite as a new phase, coexisting with nepheline, mullite, and cristobalite. For all samples, the background halo became less intense after alkaline activation. This fact indicates that the amorphous clay components produced in the first calcination were transformed into $NaAlSiO_4$ polymorphs (nepheline and low-carnegieite) due to Na_2CO_3 action [21].

Furthermore, Na_2CO_3 calcination at 800 °C and 960 °C reduced the XRD intensities corresponding to quartz, while kaolinite peaks were still present at 800 °C and 960 °C. Small reflections corresponding to a non-reacting fraction of Na_2CO_3 (PDF# 37-0451) were additionally detected in the treated clay.

3.3. Zeolite transformation

3.3.1. Crystallization from batch composition type X

Synthesis conditions for the hydrothermal conversion of samples C5X, C6X, C7X, and C8X were adjusted to promote the synthesis of NaX zeolite.

Fig. 4 shows the evolution of the X-ray diffraction patterns of samples C5X and C6X, pretreated at lower temperatures (800 °C and 960 °C, respectively). As expected, the reflections corresponding to Na_2CO_3 decreased markedly after the ageing step. For both samples, the monitoring of the reaction by XRD allowed the detection of remaining quartz and a fraction of unreacted nepheline during the whole transformation.

The growth of zeolitic crystals was clearly evidenced after 3 h of hydrothermal reaction. For the zeolitization of C5X, although the molar ratios were adjusted for obtaining NaX zeolite ($Na_{88}Al_{88}Si_{104}O_{384}{\cdot}220H_2O$, PDF# 39-0218), the diffraction patterns exhibited the formation of NaA ($Na_{96}Al_{96}Si_{96}O_{384}{\bullet}216\ H_2O$, PDF# 39-0222) as the main zeolitic component. The preferential formation of zeolite A could be attributed to the high aluminum availability promoted by the amorphous fraction generated after the pretreatments.

For sample C6X, the transformation into zeolite X was complete at 3 h of reaction. The pre-mullite formation reduced the alumina reactivity, and the treated clay was converted into the more siliceous FAU structure, a material characterized by a Si/Al molar ratio higher than 1 and lower in aluminum content compared to zeolite A. Extended times showed the reflections of both zeolites, NaA and NaX. Furthermore, low-

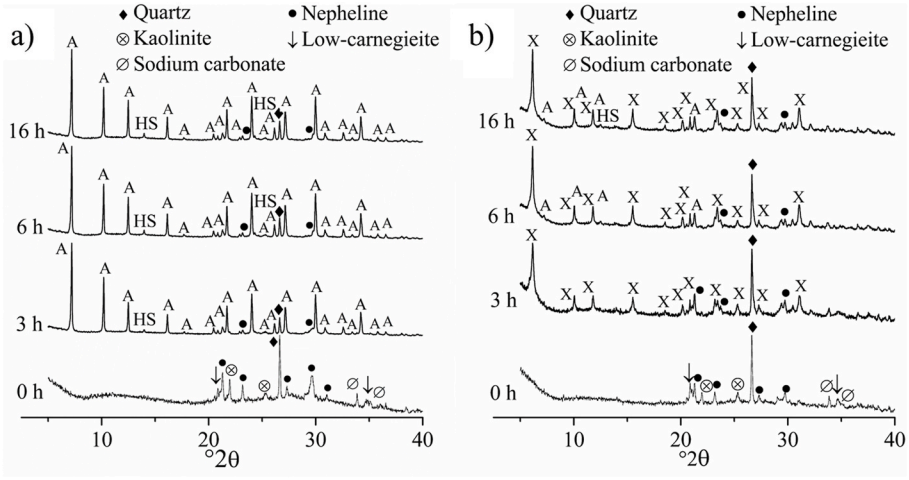

Fig. 4. Diffraction patterns obtained at 0, 3, 6, and 16 h of reaction for samples (a) C5X and (b) C6X. A: zeolite NaA, X: zeolite NaX, HS: zeolite hydroxysodalite.

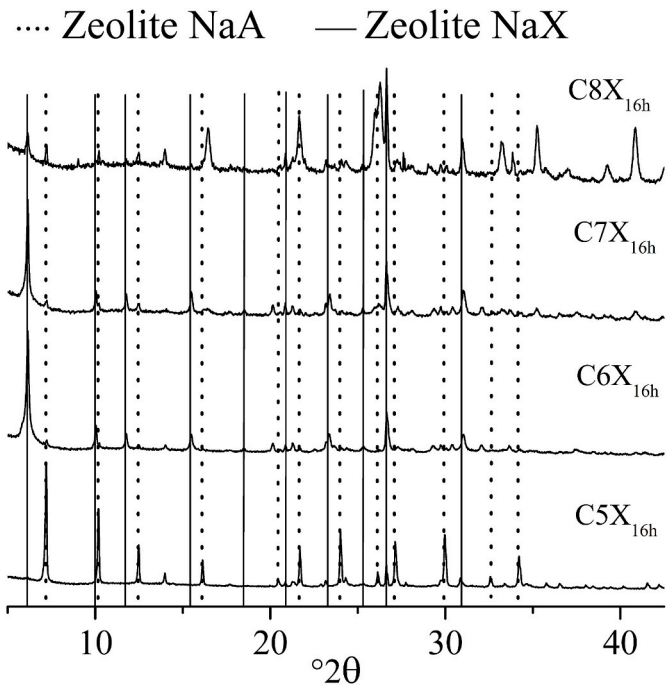

Fig. 5. Diffraction patterns obtained after 16 h of hydrothermal crystallization from batch composition type X.

intensity peaks of hydroxysodalite (PDF #42-0216) were found in the X-ray diffraction patterns of $C5A_{3h}$ and $C6A_{16h}$.

For samples C7X and C8X, the XRD analysis (not shown) indicated the formation of a mixture of X and A from the beginning of the hydrothermal reaction. Besides, reflections associated with the presence of mullite and quartz remained constant throughout the synthesis process. Particularly, relatively minor conversions into zeolite products were obtained due to the stable aluminosiliceous arrangement provided by mullite, which reduces the availability of Si and Al for constructing the FAU or LTA frameworks.

An in-depth look at the X-ray diffraction patterns for all the samples after 16 h of crystallization (Fig. 5) allowed corroborating that the $NaAlSiO_4$ polymorphs presented different stability against the alkaline conditions of the synthesis reaction: nepheline reflections were found in all samples, while those corresponding to low-carnegieite disappeared after 3 h of reaction.

3.3.2. *Crystallization of batch composition type A*

Synthesis conditions for the hydrothermal conversion of samples C5A, C6A, C7A, and C8A were adjusted to promote the crystallization of zeolite NaA. It was observed that in all the samples, NaA was identified as the main zeolitic product coexisting with other minor phases (zeolite X, P, and HS) whose appearance depended on the progress of the reaction. This synthesis evolution can be appreciated in Fig. 6, where the X-ray diffraction patterns obtained at different reaction times for samples C5A and C8A, pretreated at the minimum and maximum temperatures (800 °C and 1200 °C, respectively), are shown.

It is worth noting that zeolite formation was affected by the temperature used in the initial calcination pretreatment (Fig. 6). Comparing the X-ray diffraction patterns obtained at 3 h of reaction (Figs. 6a and 3h) it is clearly observed that C5A showed intense NaA reflections, while NaA crystallization was not observed in C8A (Figs. 6b and 3h). Similarly to the evolution noted in the zeolite X crystallization, the mullite and premullite formation occurring at high-temperature activations

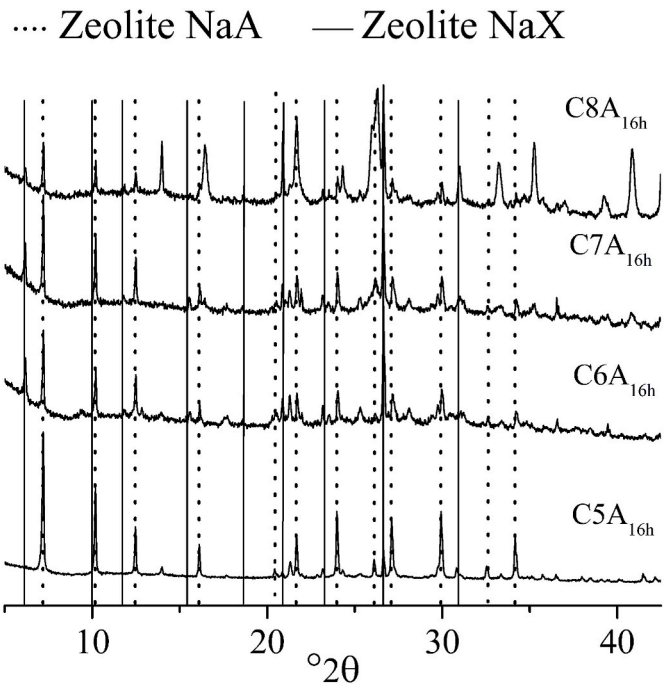

Fig. 7. Diffraction patterns obtained after 16 h of hydrothermal crystallization from batch composition type A.

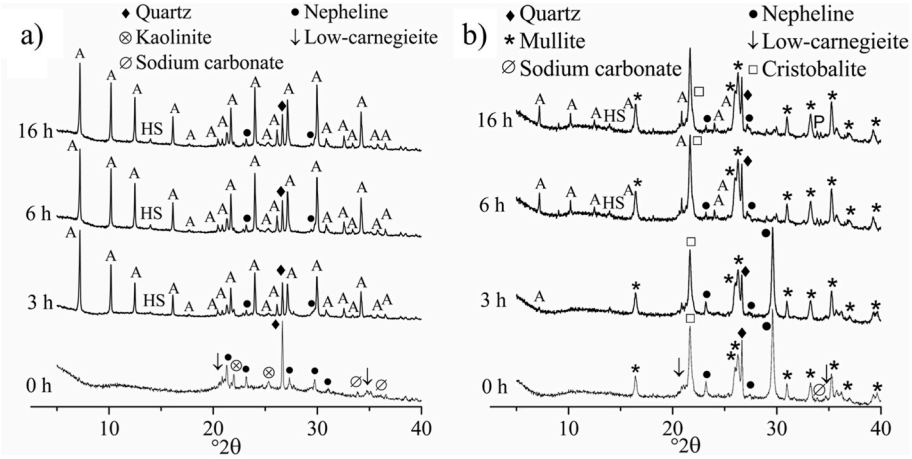

Fig. 6. Diffraction patterns obtained at 0, 3, 6, and 16 h of reaction for samples (a) C5A and (b) C8A. A: zeolite NaA, HS: hydroxysodalite, P: zeolite P.

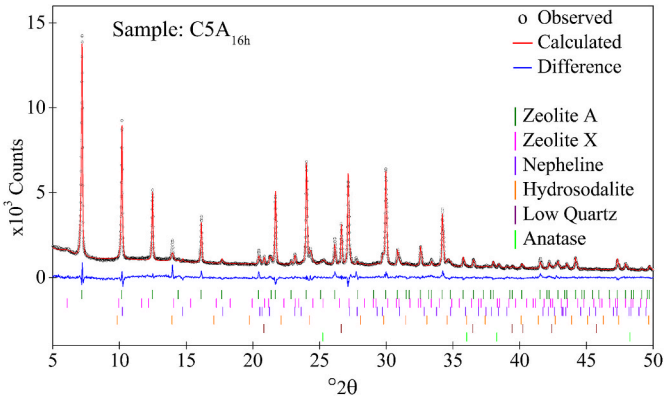

Fig. 8. Rietveld refinement of sample $C5X_{16h}$, with thermal pretreatment of 800 °C and obtained at 16 h of hydrothermal reaction.

provides physical hardness properties to the clay grains but reduces the availability of the silicon and aluminum nutrients needed for the subsequent zeolitization, retarding the hydrothermal crystallization.

Also, the quartz present in the clay as well as the mullite and cristobalite formed after calcination at 1200 °C remained unchanged during the hydrothermal transformation. Besides, as occurs in the crystallization of batch composition type X, the reflections of sodium carbonate decreased after the ageing stage.

After 16 h of reaction, the production of NaA zeolite as an exclusive phase was only obtained starting from C5A, while the other samples generated zeolite mixtures A and X. Fig. 7 shows XRD analysis for the samples C5A to C8A, at 16 h of hydrothermal reaction. Also, the presence of low-intensity reflections of hydroxysodalite and zeolite P was observed, indicating the beginning of a further transformation of the metastable structures NaX and NaA into NaP and HS.

It was very interesting to note that from the analysis of the diffraction patterns obtained after the alkaline activation step (Fig. 3), sample C5 contains nepheline, low-carnegieite, and a high halo of amorphous material. These compounds were not found in sample $C5_{16h}$. It can be inferred that the mentioned components undoubtedly acted as available sources of aluminum and silica for zeolite growth, increasing the stoichiometric Al_2O_3/SiO_2 ratio, favoring NaA zeolite crystallization. Contrarily, above 960 °C, aluminum was retained in the pre-mullite and mullite structures, diminishing the Al_2O_3/SiO_2 ratio and conducting the synthesis towards the formation of NaX and zeolite mixtures.

3.4. Zeolite quantification

As an example of the quantification data obtained, the experimental and calculated powder diffraction profiles of $C5X_{16h}$ are shown in Fig. 8.

Crystalline peaks corresponding to calcium-containing species were absent. Quartz and mullite were quantified in all samples, ratifying their resistance to zeolitization. The prevalence of nepheline changed during the course of the reaction. Besides, a low proportion of hydroxysodalite was observed.

The component weight percentages of samples C5X, C6X, C7X, and C8X at 3, 6, and 16 h of reaction time are summarized in Table 3. Weighted profile R-factor (Rwp) and goodness-of-fit (Gof) fit well with the experimental data [27].

Starting from sample $C5X_{3h}$, the crystallization of NaA proceeded very fast, resulting in a product containing NaA as the main product (83.2%) after 3 h of hydrothermal reaction. At longer reaction times, the generation of NaX and HS zeolites was favored. The starting mixture composition in this case was formulated using the molar ratios recommended for obtaining NaX zeolite, therefore it can be assumed that the effective chemical ratios in the initial mixture differed from those

Table 3
Weight percentage (wt%) of crystalline phases obtained from mixture X at 3, 6, and 16 h.

Sample	NaA	NaX	Na-P1	Nepheline	Hydroxysodalite	Other phases	Rwp	Gof
$C5X_{3h}$	83.2	–	–	9.2	5.4	2.2	6.01	1.69
$C5X_{6h}$	83.9	–	–	6.1	8.6	1.4	6.25	1.80
$C5X_{16h}$	84.8	0.7	–	4.4	8.7	1.4	5.86	1.71
$C6X_{3h}$	–	12.4	–	50.5	–	37.1	6.83	1.93
$C6X_{6h}$	7.0	22.7	–	38.5	–	31.8	8.46	2.47
$C6X_{16h}$	15.0	21.2	–	26.6	15.9	21.3	10.18	2.97
$C7X_{3h}$	2.9	2.9	–	15.3	1.3	77.6	6.38	1.71
$C7X_{6h}$	7.9	4.1	–	9.9	10.0	68.1	6.25	1.70
$C7X_{16h}$	11.9	6.3	2.5	7.8	15.6	55.9	7.61	2.13
$C8X_{3h}$	9.7	0.9	9.4	5.3	7.1	67.6	6.89	1.8
$C8X_{6h}$	8.6	0.7	5.0	2.9	4.8	78	6.74	1.84
$C8X_{16h}$	7.9	0.6	3.6	2.5	10.2	75.2	4.99	1.37

Table 4
Weight percentage (wt%) of crystalline phases obtained from mixture A at 3, 6, and 16 h.

Sample	NaA	NaX	Na-P1	Nepheline	Hydroxysodalite	Other phases	Rwp	Gof
$C5A_{3h}$	83.4	–	–	7.0	3.7	5.9	6.19	1.75
$C5A_{6h}$	88.9	–	–	4.0	2.6	4.5	5.77	1.7
$C5A_{16h}$	88.6	–	–	4.3	4.0	3.1	5.26	1.52
$C6A_{3h}$	36.0	–	–	21.4	10.3	32.3	5.77	1.59
$C6A_{6h}$	45.3	–	–	18.4	8.1	28.2	4.98	1.39
$C6A_{16h}$	44.2	0.5	11.3	12.5	7.5	24.0	5.04	1.43
$C7A_{3h}$	4.2	–	–	28.8	–	67	6.43	1.7
$C7A_{6h}$	15.5	–	–	13.0	–	71.5	6.36	1.77
$C7A_{16h}$	29.5	1.5	8.3	9.5	–	51.2	5.24	1.45
$C8A_{3h}$	2.3	–	–	12.7	–	85	14.19	3.57
$C8A_{6h}$	12.8	–	4.8	7.1	–	75.3	5.73	1.55
$C8A_{16h}$	18.9	0.4	11.2	1.8	5.9	61.8	6.32	1.72

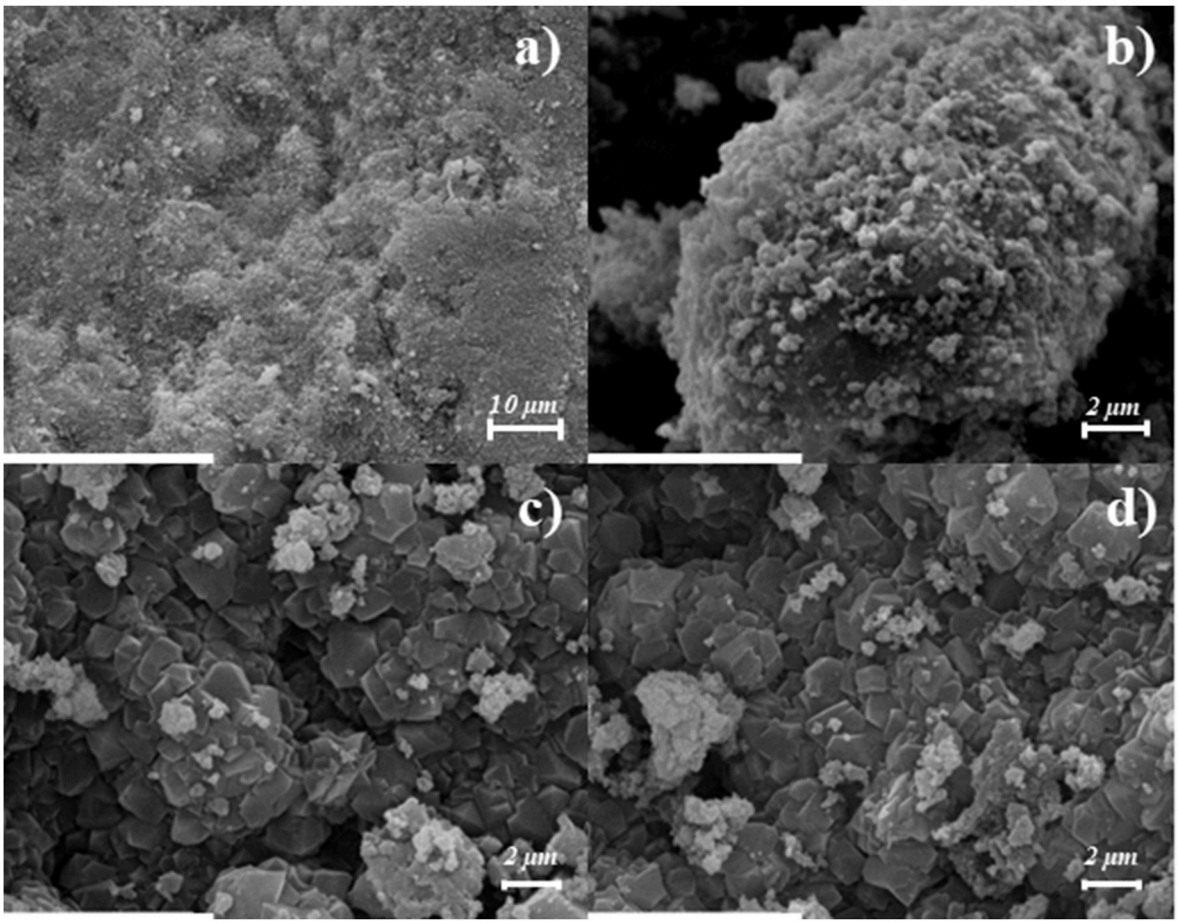

Fig. 9. SEM micrographs of selected solid samples. (a) original clay C0, X1000; (b) pretreated clay, X5000; (c) sample $C6X_{6h}$, X4000; and (d) sample $C5A_{6h}$, X4000.

theoretically estimated. Sample C6X contained NaX type zeolite only when the reaction time was 3 h; as time increased, the production of NaA was evident. For C7X and C8X samples, zeolitic mixtures were quantified including the production of Na-P1 zeolite.

The maximum zeolite conversion for NaX was achieved in sample $C6X_{16h}$, which contains 21.2% of NaX zeolite and 15% of NaA zeolite. This result confirmed that the high content of mullite modifies not only the zeolite phase distribution but also the elapsed time for an appreciable crystallization.

Table 4 lists the weight percentages obtained from the crystalline refinement of samples C5A, C6A, C7A, and C8A. For samples thermally pretreated at 800 °C, NaA was readily formed, 83.4% of NaA was detected after 3 h of hydrothermal reaction. The conversion was quite similar to that achieved for sample $C5X_{3h}$, reaching 88.6% at 16 h of reaction. In samples C6A, C7A, and C8A, the conversion into NaA increased with the reaction time, and a slight crystallization of NaX, HS, and NaP1 zeolites was verified for relatively longer times. As was described before, the high mullite content in samples C7A and C8A could affect the zeolitization process by altering silica and alumina availability.

3.5. Morphological transformation

The starting clay and samples after the pretreatment and hydrothermal steps were characterized by SEM (Fig. 9). Natural clay consisted of particles with no defined shape and size. The surface showed high roughness and also small adhering particle aggregates, Fig. 9a.

The morphological change of the natural clay after calcination and alkaline activation can be observed in Fig. 9b. After being heated at 1100 °C, the surface of the clay grains was notoriously modified. A significant growth of new small entities attached to the external surface of the original grains was observed. This new surface feature could be the result of the previously mentioned heating-induced topotactic transformation.

Furthermore, samples C5 and C6 underwent different morphological changes after the hydrothermal treatment. The clay surface was covered with cubic zeolitic crystals, corroborating that the applied pretreatments facilitated the conversion of intermediate phases into zeolites. Particularly, in samples $C6X_{6h}$ (Fig. 9c) and $C5A_{6h}$ (Fig. 9d), the entire surface of the clay was covered by zeolitic crystals, justifying the high zeolite conversions obtained, almost reaching 90% in sample $C5A_{6h}$ (Fig. 9d). It is important to note that an intergrowth of zeolite NaA and NaX crystals was observed, with a size on the order of 1–1.5 μm.

Table 5
Evolution of [Cd(II)] in the aqueous phase at 25 °C.

Time (min)	S/L = 1	S/L = 3	S/L = 3
	40 ppm	40 ppm	120 ppm
0	40	40	120
1	3.6	3.2	9.3
5	3.1	2.8	5.8
20	2.8	2.1	4.2
60	2.1	1.6	3.8
120	1.5	1.3	3.1
150	–	–	2.7
24 h	–	–	2.5

Table 6
Evolution of [Ni(II)] in the aqueous phase at 25 °C.

Time (min)	S/L = 1	S/L = 3	S/L = 3
	40 ppm	40 ppm	120 ppm
0	40	40	120
1	6.7	4.9	67
5	3.8	2,5	53
20	2.2	1.6	42
60	1.7	1.1	23
120	1.3	0.8	9.6
150	0.6	–	7.5
24 h	–	–	6.2

3.6. Cation exchange

In order to evaluate the potential application of the zeolitized products, sample $C5A_{6h}$ (presenting the highest conversion to zeolite A) was used to estimate the cadmium and nickel removal from aqueous solutions.

Tables 5 and 6 show the evolution of cadmium and nickel concentrations in the liquid phase during the ion exchange experiments.

According to these results, the concentration of both metals in the solution decreases significantly at short exchange times. As expected, the cation exchange for both metals becomes faster and more effective at the higher solid/liquid ratio. In the first minute, the amount of cadmium decreased to 3.6 ppm when 1 g of zeolite was used (Table 5, column S/L = 1, 40 ppm) and to 3.2 ppm (Table 5, column S/L = 3, 40 ppm) for 3 g of zeolite. Regarding the nickel exchange, after only 1 min the metal concentration was reduced to 6.7 ppm using 1 g of zeolite (Table 6, column S/L = 1, 40 ppm) and to 4.9 ppm for 3 g of zeolite (Table 6, column S/L = 1, 40 ppm). After 150 min, 100% removal efficiency was reached for both cations.

In relation to the tests carried out using a higher concentration (120 ppm), the results also showed appreciable metal removals at short exchange times. After 1 min, the Ni concentration decreased to 67 ppm (Table 5, column S/L = 3, 120 ppm), while the Cd concentration markedly decreased to 9.3 ppm (Table 6, column S/L = 3, 120 ppm). At 150 min, 98% and 94% removal efficiency was reached for cadmium and nickel, respectively. It is observed that high removal percentages were achieved in all cases, comparable to those reported in Ref. [28], in which a synthesized zeolite obtained from fly ash was used. The pH of the initial cadmium and nickel solutions was 3.5–4. It is worthy to note that as the different exchange experiments occurred, the pH increased up to values always below 7. It is inferred that precipitation of cadmium and nickel could rarely occur.

These results are promising, the products obtained in this way could be used directly for adsorption in packed bed columns, ensuring the mechanical stability of the material and minimizing pressure drop. Studies about the in-use mechanical stability of the synthesized particles along with the evaluation of their efficiency as ion exchange materials in a fixed adsorption bed are in progress.

4. Conclusions

The procedure presented in this work could be considered as a general methodology for obtaining hardened millimeter-sized clay particles covered by an adsorbent zeolitic coating.

The pretreatments applied to the clay take advantage of different transformation routes belonging to these kaolinite-based materials, which comprise dehydration, generation of metastable phases, and T-O-bond rearrangement, including structural collapse. The results suggest that high conversions of zeolite NaA and NaX can be achieved under suitable conditions. The high efficiency obtained in the removal of Cd^{2+} and Ni^{2+} indicates that it would be possible to use these millimeter-sized solids in packed bed-columns for pollutants adsorption. Studies about the mechanical stability of the hard-core/zeolitized shell obtained and their evaluation as ion exchange materials in a fixed adsorption bed are in progress.

Author contributions

Rivera Enríquez Claudia E.: Investigation and formal analysis. Writing: original draft. Software. **Gonzalez Maximiliano R.:** Conceptualization. Investigation and formal analysis. Writing: original draft, reviewing & editing. **Barraqué Facundo:** Resources. Visualization. **Pereyra Andrea M.:** Writing: original draft, reviewing & editing. **Basaldella Elena I.:** Conceptualization. Writing: original draft, reviewing & editing. Supervision. Project administration.

Declaration of competing interest

The authors declare that they have no known competing financial interests or personal relationships that could have appeared to influence the work reported in this paper.

Acknowledgment

C. E. Rivera-Enríquez thanks Secretaría de Educación, Ciencia, Tecnología e Innovación de la Ciudad de México (SECTEI) for the post-doctoral scholarship assigned (SECTEI/141/2019) and the Crystal Structure Refinement Laboratory at IF-UNAM for the technical support provided. M. R. Gonzalez acknowledges the financial support received from FONCyT (PICT 2017-3454).

References

[1] Henry E. Mgbemere, Ikenna C. Ekpe, Ganiyu I. Lawal, Zeolite synthesis, characterization and application areas: a review, Int. Res. J. Environ. Sci. 6 (2017) 45–59.
[2] T. Abdullahi, Z. Harun, M.H.D. Othman, A review on sustainable synthesis of zeolite from kaolinite resources via hydrothermal process, Adv. Powder Technol. 28 (2017) 1827–1840, https://doi.org/10.1016/j.apt.2017.04.028.
[3] T. Fukasawa, K. Otsuka, T. Murakami, T. Ishigami, K. Fukui, Synthesis of zeolites with hierarchical porous structures using a microwave heating method, Colloids Interface Sci. Commun. 42 (2021) 2–6, https://doi.org/10.1016/j.colcom.2021.100430.
[4] E.I. Basaldella, A. Kikot, E. Pereira, Synthesis of zeolites from mechanically activated kaolin clays, React. Solid 8 (1990) 169–177, https://doi.org/10.1016/0168-7336(90)80017-E.
[5] Y. Gu, X. Wang, Z. Qin, S. Mintova, X. Liu, Intra-crystalline mesoporous ZSM-5 zeolite by grinding synthesis method, Microporous Mesoporous Mater. 306 (2020) 1–6, https://doi.org/10.1016/j.micromeso.2020.110437.
[6] W.R. Lim, C.H. Lee, S.Y. Hamm, Synthesis and characteristics of Na-A zeolite from natural kaolin in Korea, Mater. Chem. Phys. 261 (2021), 124230, https://doi.org/10.1016/j.matchemphys.2021.124230.
[7] B.C. Amoni, A.D.L. Freitas, R.A. Bessa, C.P. Oliveira, M. Bastos-Neto, D.C. S. Azevedo, S.M.P. Lucena, J.M. Sasaki, J.B. Soares, S.A. Soares, A.R. Loiola, Effect of coal fly ash treatments on synthesis of high-quality zeolite A as a potential additive for warm mix asphalt, Mater. Chem. Phys. 275 (2022), 125197, https://doi.org/10.1016/j.matchemphys.2021.125197.
[8] J.D. Monzón, M.R. Gonzalez, M. Muñoz, A.M. Pereyra, E.I. Basaldella, PHASE-TRANSITION process in the hydrothermal zeolitization of volcanic ash into LTA and FAU structures, Clay Clay Miner. 69 (2021) 735–745, https://doi.org/10.1007/s42860-021-00148-3.
[9] M. Sayehi, G. Garbarino, G. Delahay, G. Busca, H. Tounsi, Synthesis of high value-added Na–P1 and Na-FAU zeolites using waste glass from fluorescent tubes and aluminum scraps, Mater. Chem. Phys. 248 (2020) 2–10, https://doi.org/10.1016/j.matchemphys.2020.122903.
[10] C.G. Flores, H. Schneider, J.S. Dornelles, L.B. Gomes, N.R. Marcilio, P.J. Melo, Synthesis of potassium zeolite from rice husk ash as a silicon source, Clean. Eng. Technol. 4 (2021), 100201, https://doi.org/10.1016/j.clet.2021.100201.
[11] D.L. Corwin, S.A. Bradford, Environmental impacts and sustainability of degraded water reuse, J. Environ. Qual. 37 (2008), https://doi.org/10.2134/jeq2008.0210.S-1-S-7.
[12] R. Shrinkhal, Chapter 22 - economics, technology, and environmental protection: a critical analysis of phytomanagement, in: V.C. Pandey, K. Bauddh (Eds.), Phytomanagement of Polluted Sites, Elsevier, 2019, pp. 569–580, https://doi.org/10.1016/B978-0-12-813912-7.00022-3.
[13] R.A. Rayan, M. Choudhury, M. Deb, A. Chakravorty, R.M. Devi, J. Mehta, Chapter 10 - climate change: impact on waterborne infectious diseases, in: B. Thokchom, P. Qiu, P. Singh, P.K. Iyer (Eds.), Water Conserv. Era Glob. Clim. Chang., Elsevier, 2021, pp. 213–228, https://doi.org/10.1016/B978-0-12-820200-5.00014-2.

[14] S. El-Nahas, A.I. Osman, A.S. Arafat, A.H. Al-Muhtaseb, H.M. Salman, Facile and affordable synthetic route of nano powder zeolite and its application in fast softening of water hardness, J. Water Proc. Eng. 33 (2020), https://doi.org/10.1016/j.jwpe.2019.101104.
[15] A. Rozhkovskaya, J. Rajapakse, G.J. Millar, Process engineering approach to conversion of alum sludge and waste glass into zeolite LTA for water softening, J. Water Proc. Eng. 43 (2021), https://doi.org/10.1016/j.jwpe.2021.102177.
[16] O.A. Odunlami, D.A. Vershima, T.E. Oladimeji, S. Nkongho, S.K. Ogunlade, B. S. Fakinle, Advanced techniques for the capturing and separation of CO 2 – a review, Results Eng. 15 (2022), 100512.
[17] V. Kavitha, Global prevalence and visible light mediated photodegradation of pharmaceuticals and personal care products (PPCPs)-a review, Results Eng. 14 (2022), 100469, https://doi.org/10.1016/j.rineng.2022.100469.
[18] E.T. Wahyuni, N.P. Diantariani, I. Kartini, A. Kuncaka, Enhancement of the photostability and visible photoactivity of ZnO photocatalyst used for reduction of Cr(VI) ions, Results Eng. 13 (2022) 18–21, https://doi.org/10.1016/j.rineng.2022.100351.
[19] J. Jjagwe, P.W. Olupot, E. Menya, H.M. Kalibbala, Synthesis and application of granular activated carbon from biomass waste materials for water treatment: a review, J. Bioresour. Bioprod. 6 (2021) 292–322, https://doi.org/10.1016/j.jobab.2021.03.003.
[20] R. de' Gennaro, P. Cappelletti, G. Cerri, M. de' Gennaro, M. Dondi, G. Guarini, A. Langella, D. Naimo, Influence of zeolites on the sintering and technological properties of porcelain stoneware tiles, J. Eur. Ceram. Soc. 23 (2003) 2237–2245, https://doi.org/10.1016/S0955-2219(03)00086-4.
[21] J.D. Monzón, M.R. Gonzalez, L.E. Mardones, M.S. Conconi, A.M. Pereyra, E. I. Basaldella, The role of alkaline activation in the structural transformations of aluminosiliceous industrial wastes towards zeolite production, Mater. Today Commun. 21 (2019), https://doi.org/10.1016/j.mtcomm.2019.100624.
[22] H.M. Rietveld, A profile refinement method for nuclear and magnetic structures, J. Appl. Crystallogr. 2 (1969) 65–71, https://doi.org/10.1107/S0021889869006558.
[23] J.A. Pask, A.P. Tomsia, Formation of mullite from sol-gel mixtures and kaolinite, J. Am. Ceram. Soc. 74 (1991) 2367–2373, https://doi.org/10.1111/j.1151-2916.1991.tb06770.x.
[24] K.F. Jusnes, M. Tangstad, E. Ringdalen, Phase transformations from quartz to cristobalite, in: B.R. Davis, M.S. Moats, S. Wang, D. Gregurek, J. Kapusta, T. P. Battle, M.E. Schlesinger, G.R. Alvear Flores, E. Jak, G. Goodall, M.L. Free, E. Asselin, A. Chagnes, D. Dreisinger, M. Jeffrey, J. Lee, G. Miller, J. Petersen, V.S. T. Ciminelli, Q. Xu, R. Molnar, J. Adams, W. Liu, N. Verbaan, J. Goode, I. M. London, G. Azimi, A. Forstner, R. Kappes, T. Bhambhani (Eds.), Extr. 2018, Springer International Publishing, Cham, 2018, pp. 717–727.
[25] H. Schneider, A. Majdic, R. Vasudevan, Kinetics of the quartz-cristobalite transformation in refractory- grade silica materials, Mater. Sci. Forum 7 (1986) 91–102. https://dx.doi.org/10.4028/www.scientific.net/msf.7.91.
[26] A.K. Chakravorty, D.K. Ghosh, Kaolinite–mullite reaction series: the development and significance of a binary aluminosilicate phase, J. Am. Ceram. Soc. 74 (1991) 1401–1406, https://doi.org/10.1111/j.1151-2916.1991.tb04119.x.
[27] B.H. Toby, R factors in Rietveld analysis: how good is good enough? Powder Diffr. 21 (2006) 67–70, https://doi.org/10.1154/1.2179804.
[28] M. Visa, Synthesis and characterization of new zeolite materials obtained from fly ash for heavy metals removal in advanced wastewater treatment, Powder Technol. 294 (2016) 338–347, https://doi.org/10.1016/j.powtec.2016.02.019.